



# Grifolamine A, a novel bis- $\gamma$ -butyrolactone from *Grifola frondosa* exerted inhibitory effect on $\alpha$ -glucosidase and their binding interaction: Affinity and molecular dynamics simulation

Shaodan Chen<sup>a,1</sup>, Zhenqiang Mu<sup>b,1</sup>, Tianqiao Yong<sup>a</sup>, Jiangyong Gu<sup>c</sup>, Yifan Zhang<sup>a</sup>, Xiong Gao<sup>a</sup>, Yizhen Xie<sup>a</sup>, Chun Xiao<sup>a</sup>, Huiping Hu<sup>a</sup>, Xiaobing Yang<sup>a</sup>, Xiangmin Li<sup>a</sup>, Manjun Cai<sup>a</sup>, Qingping Wu<sup>a,\*</sup>

<sup>a</sup> State Key Laboratory of Applied Microbiology Southern China, Guangdong Provincial Key Laboratory of Microbial Safety and Health, Key Laboratory of Agricultural Microbiomics and Precision Application, Ministry of Agriculture and Rural Affairs, Guangdong Institute of Microbiology, Guangdong Academy of Sciences, Guangzhou, 510070, China

<sup>b</sup> Chongqing Engineering Research Center of Pharmaceutical Sciences, Chongqing Medical and Pharmaceutical College, Chongqing, 410331, China

<sup>c</sup> Research Centre for Integrative Medicine, School of Basic Medical Science, Guangzhou University of Chinese Medicine, Guangzhou, 510006, China

## ARTICLE INFO

### Keywords:

Grifolamine A  
Bis- $\gamma$ -butyrolactone  
 $\alpha$ -glucosidase  
*Grifola frondosa*  
Absolute configuration  
Surface plasmon resonance  
Molecular dynamics simulation

## ABSTRACT

A novel bis- $\gamma$ -butyrolactone grifolamine A (**1**), the first  $\gamma$ -butyrolactone dimer from nature, together with three known  $\gamma$ -butyrolactones (**2–4**), was isolated from the byproduct from *Grifola frondosa* polysaccharides preparation process. The structure and stereochemistry of grifolamine A (**1**) were elucidated by extensive spectroscopic analysis combined with quantum chemical calculation. The biosynthetic origin of compound **1**, as well as **2–4** was proposed. Grifolamine A (**1**) showed an intense inhibition against  $\alpha$ -glucosidase *in vitro*. The underlying inhibitory mechanism was revealed by surface plasmon resonance (SPR), molecular docking, molecular dynamics (MD) simulation and binding free energy calculation. SPR revealed that grifolamine A exhibited a strong affinity to  $\alpha$ -glucosidase with an equilibrium dissociation constant ( $K_D$ ) value of  $1.178 \times 10^{-4}$  M. Molecular docking manifested that grifolamine A sat at the active pocket of  $\alpha$ -glucosidase by van der Waals force, alkyl interaction and carbon hydrogen bonds, and consequently changed the micro-environmental structure of  $\alpha$ -glucosidase. MD simulation revealed that grifolamine A had high binding affinity to  $\alpha$ -glucosidase with average free energy of  $-25.2 \pm 3.2$  kcal/mol. Free energy decomposition indicated amino acid residues including PHE298, PHE308, PHE309, PHE155 and ARG310 at the binding pocket played a strongly positive effect on the interaction between grifolamine A and  $\alpha$ -glucosidase. Our findings provide valuable information for the design and development of novel  $\alpha$ -glucosidase inhibitors based on  $\gamma$ -butyrolactone skeleton.

## 1. Introduction

Type 2 diabetes mellitus (T2DM), featured with hyperglycemia, has become one of the major international public health events (Miao et al., 2022). Postprandial hyperglycemia is a key characteristic of T2DM and was positively associated with such complications as cardiovascular diseases (Araujo et al., 2021). Fortunately, postprandial hyperglycemia can be effectively improved by inhibiting the carbohydrate hydrolases such as  $\alpha$ -glucosidase located in the small intestinal tract. Inhibiting  $\alpha$ -glucosidase can not only delay the hydrolysis of carbohydrates into

saccharides which were absorbed into blood, thereby controlling postprandial blood glucose, but also protect the islet  $\beta$  cell function and alleviate T2DM and associated complications (Luis Ros, Francini and Schinella, 2015; Sun and Miao, 2020). Acarbose, an  $\alpha$ -glucosidase inhibitor, has been used as the first-line medicine for the treatment of T2DM, especially for patients who consumed a high-carbohydrate diet, however, the side effects on gastrointestinal digestion restricted its long-term use (Suttithumsatid et al., 2022). Thus, searching for safer inhibitors suitable for long-term use is urgent.

The edible mushroom *Grifola frondosa*, also known as maitake, has

\* Corresponding author. Guangdong Institute of Microbiology, No. 100 Xianlie Rd, Guangzhou, China.

E-mail address: [wuqp203@163.com](mailto:wuqp203@163.com) (Q. Wu).

<sup>1</sup> These authors contributed equally to this work.

<https://doi.org/10.1016/j.crfs.2022.10.026>

Received 13 August 2022; Received in revised form 19 October 2022; Accepted 26 October 2022

Available online 27 October 2022

2665-9271/© 2022 Published by Elsevier B.V. This is an open access article under the CC BY-NC-ND license (<http://creativecommons.org/licenses/by-nc-nd/4.0/>).

been used as a food delicacy and a traditional dietary nutritional supplement for a long history in Asian countries. Over the last few decades, accumulated evidences demonstrated that *G. frondosa* had outstanding pharmacological properties including hypoglycemic, hypolipidemic, anti-tumor, and immunomodulatory (Li et al., 2022; Mizuno et al., 2017; Ouyang et al., 2022; Zhang et al., 2022). These bioactivities might be attributed to its multiple metabolites including polysaccharides, sterols, ceramides and alkaloids (Chen et al., 2018; Meng et al., 2017; Yaoita et al., 2000; A. Zhang, Deng, Yu, Zhang, Linhardt and Sun, 2018).

Previously, in our investigation on biologically active constituents from *G. frondosa*, we firstly reported pyrrole alkaloids from *G. frondosa* exerted inhibitory effects against  $\alpha$ -glucosidase (Chen et al., 2018). As a continuing work on searching anti-diabetic agents from *G. frondosa*, we report the isolation of a novel bis- $\gamma$ -butyrolactone, named grifolamine A (1) and three known monomer  $\gamma$ -butyrolactones (2–4) (Fig. 1) from the byproduct from *G. frondosa* polysaccharides preparation process. Especially, grifolamine A (1) was the first natural  $\gamma$ -butyrolactone dimer with a characteristic feature of an N-linkage between the two  $\gamma$ -butyrolactone moieties and then the biosynthetic origin was proposed. Interestingly, the dimer grifolamine A (1) showed more intensive inhibitory activity than the three monomers (2–4) against  $\alpha$ -glucosidase, and even it was more active than the positive control acarbose. The interaction mechanism between grifolamine A and  $\alpha$ -glucosidase was further analyzed by surface plasmon resonance (SPR), molecular docking, molecular dynamics (MD) simulation and binding free energy calculation. These results would provide a research clue to the  $\gamma$ -butyrolactone dimers and polymers, as well as to the development and utilization of *G. frondosa* byproduct as functional food ingredients or natural nutraceuticals.

## 2. Materials and methods

### 2.1. General methods

1D and 2D NMR spectra were measured on a Bruker AVANCE III 600 spectrometer. ECD data were recorded in CH<sub>3</sub>OH using a JASCO J-810 spectrophotometer (Jasco International Co., Ltd., Tokyo, Japan). Optical rotation was measured on a JASCO P2000 digital polarimeter (Jasco International Co. Ltd., Tokyo, Japan). Semi-preparative HPLC was performed on a Shimadzu LC-20A spectrophotometer. YMC-Pack Pro C18 column (5  $\mu$ m, 10  $\times$  250 mm) and Octadecylsilylanized (ODS) silica gel (50  $\mu$ m) were obtained from Japan YMC Ltd.,. Rat intestinal acetone powder,  $\alpha$ -glucosidase (from yeast), *p*-nitrophenyl- $\alpha$ -D-glucopyranoside (P-NPG) and chromogenic dinitrosalicylic acid (DNS) were purchased from Sigma-Aldrich Co., LLC. Acarbose was purchased from Shanghai Yuanye Bio-Technology Co., Ltd. Amino coupling kit and CM5 chip were purchased from Cytiva.

### 2.2. Extraction and isolation

The air-dried and powdered fruiting bodies of *G. frondosa* (1.0 kg), presented by Guangdong Yuewei Edible Fungi Technology Co. Ltd., were refluxed twice with pure water for 2 h each time. After filtration,

the filtrate was concentrated under reduced pressure. The concentrated solution (GF) was added 4 times of absolute ethanol and stayed at room temperature for 48 h. The supernatant (GF-E) was collected and concentrated to remove the ethanol. The suspension (GF-E) was mixed with ethyl acetate and extracted 3 times by liquid-liquid extraction. The supernatant (GF-EE) was combined and concentrated to remove ethyl acetate.

The GF-EE fraction was applied to an ODS silica gel column eluted with MeOH–H<sub>2</sub>O (10:90, 20:80, 30:70, 50:50 and 100:0) to afford five subfractions (Fr. 1~ Fr. 5). Fr. 2 was further purified by semi-preparative HPLC (MeOH–H<sub>2</sub>O, 20:80) to afford compounds 1 (1.9 mg), 2 (2.6 mg), 3 (1.3 mg) and 4 (1.6 mg).

Grifolamine A (1): Yellow amorphous powder; Yield: 0.019%; [ $\alpha$ ]<sub>D</sub><sup>25</sup> -15.4 (c, 0.5, CH<sub>3</sub>OH); IR (KBr)  $\nu_{\max}$  3382, 2931, 2875, 1750, 1645, 1440, 1385, 1043, 951 cm<sup>-1</sup>; ECD (MeOH)  $\lambda_{\max}$  (log  $\epsilon$ ) 215 (3.03) nm; HRESIMS  $m/z$  268.1565 [M + H]<sup>+</sup> (calculated for C<sub>14</sub>H<sub>22</sub>NO<sub>4</sub>, 268.1549); <sup>1</sup>H NMR (600 MHz, in CD<sub>3</sub>OD):  $\delta_{\text{H}}$  4.86 (2H, m, H-5), 1.83 (3H, t, 1.8, H-6), 4.89 (1H, q, 6.6, H-7), 1.38 (3H, d, 6.6, H-8), 2.54 (1H, dq, 9.9, 6.6, H-3'), 2.21 (1H, m, H-4'), 4.38 (1H, t, 9.0, H-5'a), 4.15 (1H, t, 9.0, H-5'b), 1.24 (3H, d, 6.6, H-6'), 3.84 (1H, m, H-7') and 1.21 (3H, d, 6.6, H-8'); <sup>13</sup>C NMR (150 MHz, in CD<sub>3</sub>OD):  $\delta_{\text{C}}$  177.8 (s, C-2), 122.2 (s, C-3), 166.2 (s, C-4), 70.8 (t, C-5), 8.6 (q, C-6), 64.5 (d, C-7), 22.1 (q, C-8), 182.7 (s, C-2'), 37.7 (d, C-3'), 51.4 (d, C-4'), 69.1 (t, C-5'), 14.9 (q, C-6'), 67.5 (d, C-7') and 21.7 (q, C-8').

(3S, 4S)-4-acetyl-3-methyl-2-hydroxy-5-(2-hydroxy-2-methyl-2-hydrofuran-3-yl)-2-hydrofuran-3-yl-1-one (2): Light yellow powder; Yield: 0.026%; ESIMS  $m/z$  141 [M – H]<sup>-</sup>; <sup>1</sup>H NMR (600 MHz, in CD<sub>3</sub>OD):  $\delta_{\text{H}}$  2.85 (1H, m, H-3), 3.29 (1H, q, 9.6, H-4), 4.69 (1H, t, 9.0, H-5a), 4.46 (1H, t, 9.0, H-5b), 1.35 (3H, d, 7.2, H-6), and 2.27 (3H, s, H-8); <sup>13</sup>C NMR (150 MHz, in CD<sub>3</sub>OD):  $\delta_{\text{C}}$  177.7 (s, C-2), 38.7 (d, C-3), 54.9 (d, C-4), 66.4 (t, C-5), 15.9 (q, C-6), 204.2 (s, C-7), and 29.7 (q, C-8).

2-methyl-2-hydroxy-3,4-dimethyl-5-oxo-2,5-dihydrofuran (3): Light yellow powder; Yield: 0.016%; ESIMS  $m/z$  141 [M – H]<sup>-</sup>; <sup>1</sup>H NMR (600 MHz, in CD<sub>3</sub>OD):  $\delta_{\text{H}}$  1.77 (3H, d, 0.6, H-6), 1.96 (3H, d, 0.6, H-7), 1.55 (3H, s, H-8) and 4.84 (1H, s, OH); <sup>13</sup>C NMR (150 MHz, in CD<sub>3</sub>OD):  $\delta_{\text{C}}$  174.3 (s, C-2), 124.7 (s, C-3), 161.2 (s, C-4), 107.7 (s, C-5), 8.3 (q, C-6), 10.6 (q, C-7), and 23.7 (q, C-8).

Myrolactones B (4): Light yellow powder; Yield: 0.026%; ESIMS  $m/z$  157 [M – H]<sup>-</sup>; <sup>1</sup>H NMR (600 MHz, in CD<sub>3</sub>OD):  $\delta_{\text{H}}$  1.91 (3H, s, H-6), 4.46 (2H, s, H-7), and 1.65 (3H, s, H-8); <sup>13</sup>C NMR (150 MHz, in CD<sub>3</sub>OD):  $\delta_{\text{C}}$  176.2 (s, C-2), 126.6 (s, C-3), 163.0 (s, C-4), 107.2 (s, C-5), 8.8 (q, C-6), 57.3 (q, C-7) and 24.2 (q, C-8).

### 2.3. Calculations

Comparing computed electronic circular dichroism (ECD) and optical rotations (OR) with experimental results is a valid method to assign absolute configurations of natural products (Zhu, 2009, 2015). The quantum chemical calculation was performed using the Gaussian 09 Program. The geometries with low energy values were used for optimizations using the density functional theory (DFT) method at the B3LYP/6-31G (d,p) level. The optimized conformers having 0–5 kcal/mol relative energy to the lowest energy conformer were then used for

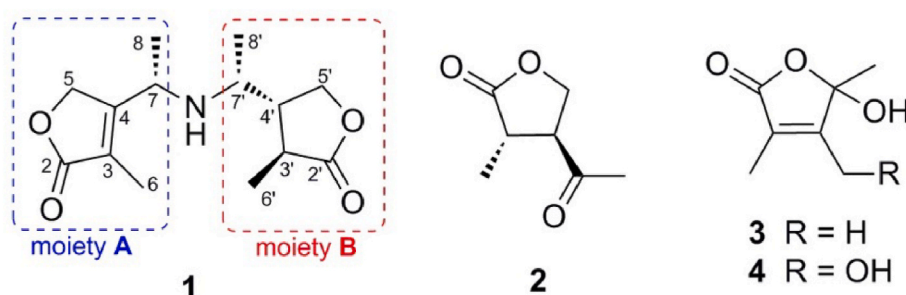


Fig. 1. Chemical structures of compounds 1–4.

further computations at the B3LYP/6–311++G (2d, p) level. The proton's distance of H6'/H8' was calculated from their optimized conformers through Boltzmann statistics. The excitation energies and rotational strengths were calculated using time-dependent density functional theory (TDDFT) at the B3LYP/6–311++G (2d, p) level (Liao et al., 2015). The ECD spectra were simulated from electronic excitation energies and velocity rotational strengths (Bobst, 1984). The specific optical rotations of the four geometries (1a–1d) were calculated with the optimized conformers at the B3LYP/6–311++G (2d, p) level at the wavelength of 589.3 nm (Fang et al., 2018). Solvent effects were considered by CPCM and methanol was selected as the solvent consistent with the experimental. Boltzmann statistics were used to simulate their corresponding values after the calculations of OR and ECD for each conformation, respectively. These simulated data were used to compare to experimental data.

#### 2.4. Inhibition assays against $\alpha$ -glucosidase from yeast and from rats' small intestinal mucosa

The inhibitory effects of compounds 1–4 on  $\alpha$ -glucosidase from yeast and rats' small intestinal mucosa were carried out according to our previous study (Chen et al., 2018). Acarbose was used as a positive control.

#### 2.5. Surface plasmon resonance (SPR) assay

SPR assay was analyzed according to our previously reported methods on a GE Biacore T200 system (Chen et al., 2022). Briefly, activated  $\alpha$ -glucosidase was immobilized on a CM5 sensor chip using an amine coupling kit. Test sample solutions were serially injected over  $\alpha$ -glucosidase coated surface. The equilibrium dissociation constant ( $K_D$ ) was calculated by the Biacore evaluation software.

#### 2.6. Molecular docking

The  $\alpha$ -glucosidase homology model had been built and validated according to our previously reported methods (Chen et al., 2021). Molecular docking simulation was performed using Gold. The diameter of the sphere centered on the centroid of copied ligand in homology modeling was set to 13 Å. Goldscore was used as a score function.

#### 2.7. Molecular dynamics (MD) simulation and binding free energy calculation

Simulations were carried out using the AMBER 16 molecular dynamics program. The docked structure of  $\alpha$ -glucosidase in complex with grifolamine A was used as the initial structure. The corresponding topology files of the ligands were generated using Antechamber module in Amber 16 and the charge distributions were assigned with the charges calculated at the DFT/6–31G\* level with the quantum method. The AMBER ff14SB force field was applied to  $\alpha$ -glucosidase, which was then solvated using the TIP3P water model at the size of 15 Å. Sodium chloride (0.15 M) was added to neutralize and salt the systems. The system was energy minimized according to the sequenced process of optimizing solvent molecules, side chains of  $\alpha$ -glucosidase and backbone of  $\alpha$ -glucosidase. And then, the temperature of the system increased gradually to 310 K. 100 ns molecular dynamics simulation was performed. Root mean square deviation (RMSD) of backbone was monitored. Obtained trajectory was used for binding free energy calculations with molecular mechanics Poisson-Boltzmann surface area (MM-PBSA) method (Aldeghi et al., 2016; Srinivasan et al., 1998). Snapshots extracted from MD trajectory were used for calculation of MM-PBSA binding free energy. All calculations of MM-PBSA were performed using the g.mmpbsa package developed from GROMACS and APBS programs (Aldeghi et al., 2016; Kumari et al., 2014).

### 3. Results and discussion

#### 3.1. Preparation and structure elucidation of compounds

Dried *G. frondosa* were extracted with water and then precipitated by alcohol to obtain the crude polysaccharides. The supernatant, which was considered as a byproduct from the alcohol precipitation, was concentrated to remove the alcohol and partitioned with ethyl acetate to extract a fraction (GF-EE). The GF-EE fraction was then separated by various chromatographic techniques to obtain compounds 1–4.

Compound 1 was obtained as a yellow amorphous powder. The molecular formula of 1 was determined as  $C_{14}H_{21}NO_4$  based on ESI-Q/TOF-MS at  $m/z$  268.1565  $[M+H]^+$  (calculated for  $C_{14}H_{22}NO_4$ , 268.1549). The  $^1H$  NMR data (in  $CD_3OD$ , 600 MHz) indicated the presences of four methyls ( $\delta_H$  1.83, t, 1.8;  $\delta_H$  1.38, d, 6.6;  $\delta_H$  1.24, d, 6.6;  $\delta_H$  1.21, d, 7.2). In the  $^{13}C$  NMR (in  $CD_3OD$ , 150 MHz) and DEPT-135 spectra, 14 carbon signals including two lactone carbonyls ( $\delta_C$  182.7 and 177.8), two olefinic quaternary carbons ( $\delta_C$  166.2 and 122.2), two methylenes ( $\delta_C$  70.8 and 69.1), four methines ( $\delta_C$  67.5, 64.5, 51.4 and 37.7), and four methyls ( $\delta_C$  22.1, 21.7, 14.9 and 8.6) were observed. The HMBIC correlations from Me-6 (1.83, t) to C-2 (177.8), C-3 (122.2), and C-4 (166.2), from H-5 (4.86) to C-3 (122.2), C-4 (166.2), and C-7 (64.5), and from Me-8 (1.38, d) to C-4 and C-7 suggested the presence of an  $\alpha$ -methyl- $\gamma$ -butenolide moiety (Fig. 2). In addition, correlations from Me-6' (1.24, d) to C-2' (182.7), C-3' (37.7), and C-4' (51.4), from H-5' (4.38, 4.15) to C-3' (37.7), C-4' (51.4), and C-7' (67.5), and from Me-8' (1.21, d) to C-4' and C-7' suggested the presence of another  $\alpha$ -methyl- $\gamma$ -butyrolactone moiety (Fig. 2).  $^1H$ - $^1H$  COSY correlations of H-7 (4.89, q)/H-8 (1.38, d), H-3-6' (1.24, d)/H-3' (2.54, dq)/H-4' (2.21, m)/H-2-5' (4.38 and 4.15, t), H-4'/H-7' (3.84, m)/H-3-8' (1.21, d) were also shown (Fig. 2). Based on the molecular formula  $C_{14}H_{21}NO_4$ , the above two moieties A and B (Figs. 1 and 2) were linked by the sole nitrogen atom. Therefore, the overall planar structure of 1, a  $\gamma$ -butyrolactone dimer with N-linkage, was established.

ROESY correlations of H-6' to H-3', H-3' to H-4', H-4' to H-5' $\alpha$ , H-4' to H-5' $\beta$ , and H-7' to H-8' were obvious (Fig. 2). The paucity of the ROESY correlations of H-3' to H-7', H-4' to H-6', and H-6' to H-8' implied that the constituent at C-4' was not at the same side as that at C-6' of moiety B. Otherwise, H-8' would be close in proximity to H-6' through a rotation of C-7' and C-4' bond and the ROESY correlation of H-6'/H-8' could be shown. In this case, the protons distance of H-6'/H-8' using the quantum chemical calculation was employed, which could be used as the corroborative evidence indirectly to confirm the proposed *trans*-orientation of moiety B. The protons distance of H-6'/H-8' in the *trans* and *cis* epimers of moiety B in 1 were calculated by DFT (B3LYP) at the 6–311++G (2d,p) level. The calculated protons distance of H-6'/H-8' in 1a (*trans*) was 5.20 Å, compared with 3.98 Å in 1a' (*cis*) (Fig. 3). Acknowledgedly, ROESY experiment correlates protons that are close to each other in space within 4.50 Å (LaPlante, Bilodeau, Aubry, Gillard, O'Meara and Coulombe, 2013; Silverstein et al., 2005). The results of the calculated protons distance were highly in accordance with the ROESY experiment. Thus, the relative configuration of C-3' and C-4' in 1 was *trans*-oriented. Since the CD spectrum showed a positive Cotton effect at 210–230 nm region, the configuration of C-3' ( $\alpha$ -carbon) in compound 1 was assigned as *S* according to the Okuda rule (Forzato et al., 2005; Forzato et al., 1997; Okuda et al., 1964), which was also confirmed by the calculated ECD spectrum using time-dependent density functional theory (TDDFT) (Fig. 4). Considering that the ECD curve of 1 was complicated by the  $n \rightarrow \pi^*$  transition bands of moiety A, which may have a disturbing effect on the determination of the configuration of C-3' in compound 1 by the Okuda rule. The ECD curve of moiety B was also calculated by the same method. The calculated results showed that the ECD spectrum of moiety B exhibited a very similar ECD curve at 210–230 nm regions to the experiment ECD spectrum of 1 and the calculated ECD spectrum of 1a. Based on these results, the absolute configuration of C-3' and C-4' in compound 1 was assigned as 3*S*, 4*S*.

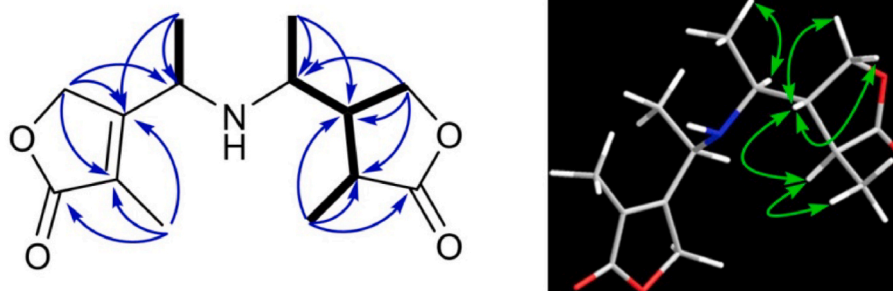
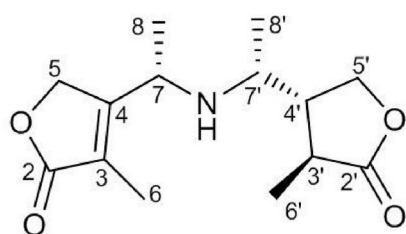
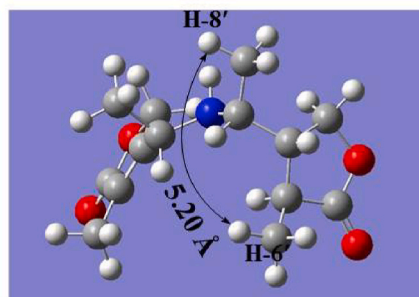


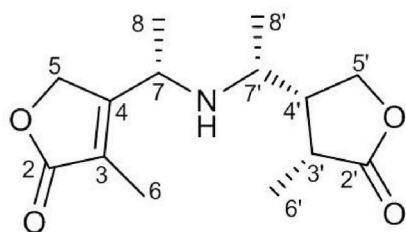
Fig. 2. Key HMBC ( $\rightarrow$ ),  $^1\text{H}$ - $^1\text{H}$  COSY ( $\blacksquare$ ) and NOESY ( $\leftrightarrow$ ) correlations of compound **1**.



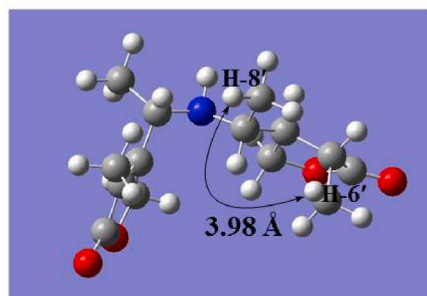
**1a**



Optimized conformation of **1a**



**1a'**



Optimized conformation of **1a'**

Fig. 3. Calculated protons distance of H-6'/H-8' in **1a** and **1a'**.

Finally, to determine the absolute configuration of C-7 and C-7', the specific optical rotation of four possible epimers proposed for **1** was calculated using DFT (B3LYP) at the 6-311++G (2d,p) level with the total four epimers **1a-1d** (Fig. 5, **1a-1d**). Amongst, the calculated value of **1a** ( $[\alpha]_D^{25}$ -15.4 (c, 0.5, CH<sub>3</sub>OH) of **1**, which suggested the C-7S and C-7'R, respectively. Thus, the stereochemistry was tentatively elucidated. Compound **1** was a novel bis- $\gamma$ -butyrolactone with N-linkage, named grifolamine A.

The known compounds (**2-4**) were identified as (3S, 4S)-4-acetyl-3-methyldihydrofuran-2(3H)-one (**2**) (Choi et al., 2014; Forzato et al., 2005), 2-methyl-2-hydroxy-3,4-dimethyl-5-oxo-2,5-dihydrofuran (**3**) (Surmont et al., 2010), and myrolactones B (**4**) (Xu et al., 2011) by comparing their  $^1\text{H}$ ,  $^{13}\text{C}$  NMR and mass data with the corresponding data in literatures. Compounds **2-4** were monomer  $\gamma$ -butyrolactones, which were also isolated from *Grifola* for the first time.

### 3.2. Proposed biosynthetic origin of grifolamine A (**1**)

The biosynthetic origin of grifolamine A (**1**), as well as the known compounds **2-4**, could be traced back to a common precursor **P**, which

formed intermediates **2** and **I<sub>4</sub>** through various cyclization modes, respectively (Scheme 1). Intermediate **2** would be transformed into **I<sub>2</sub>** via reduction,  $\alpha$ -hydroxylation, and dehydration process. Concomitantly, **2** underwent a transamination reaction to produce **I<sub>3</sub>**, an N-containing  $\gamma$ -butyrolactone, which finally yielded **1** by a nucleophilic attack of amino on to hydroxyl carbon of **I<sub>2</sub>**. This process involved a configuration inversion of the hydroxyl carbon, which explained the contrary configuration of C-7 and C-7' in **1**. Especially, the key intermediates **2**, **I<sub>1</sub>**, and **I<sub>2</sub>** had been reported from *Mycoleptodonoides aitchisonii*, an edible mushroom also (Choi et al., 2014).

### 3.3. Inhibitory effect on $\alpha$ -glucosidase

The compounds were evaluated for their inhibitory effects against  $\alpha$ -glucosidase from yeast and rats' intestines *in vitro*, using acarbose as a positive control (Table 1). The IC<sub>50</sub> value of acarbose against  $\alpha$ -glucosidase from yeast was  $656.7 \pm 17.3 \mu\text{M}$ , which was greatly different from that from rats' intestines ( $32.1 \pm 4.6 \mu\text{M}$ ). Especially, the  $\gamma$ -butyrolactone dimer grifolamine A (**1**), exhibited the strongest inhibitory activity against both  $\alpha$ -glucosidases, with IC<sub>50</sub> value of  $83.7 \pm 4.4$

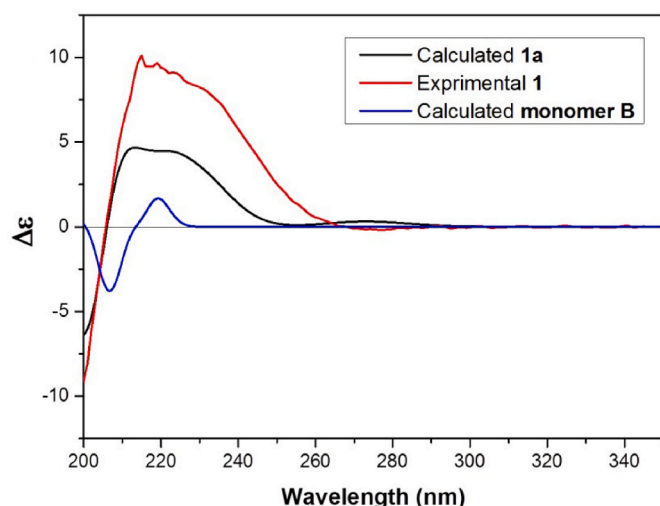


Fig. 4. Calculated and experimental ECD spectra of 1.

$\mu\text{M}$  against  $\alpha$ -glucosidase from rats' intestines and  $78.6 \pm 6.7 \mu\text{M}$  against  $\alpha$ -glucosidase from yeast, even was 8 times stronger than acarbose against  $\alpha$ -glucosidase from yeast. It is noteworthy that the  $\gamma$ -butyrolactone monomer 2 also showed more remarkable inhibition than other monomers 3 and 4, which may imply the impact of  $\beta$  and  $\gamma$  substituents.

### 3.4. SPR analysis of grifolamine A

SPR biosensor is special in the application of screening out bioactive molecules as it can measure the affinity and kinetics of bimolecular binding in a label-free fashion with low reagent consumption (Cao et al., 2022). As shown in Fig. 6, grifolamine A bound to  $\alpha$ -glucosidase in a concentration-dependent manner. The equilibrium dissociation constant ( $K_D$ ) was calculated as  $1.178 \times 10^{-4} \text{ M}$ , which disclosed that grifolamine A had a high affinity to  $\alpha$ -glucosidase.

### 3.5. Molecular docking

Molecular docking is helpful for clarifying the most energetically favorable binding site within the structure of two biomolecules (Tian et al., 2022). Fig. 7 showed the overall and close views of grifolamine A docked into the binding pocket of  $\alpha$ -glucosidase mainly through van der Waals interactions produced from the amino acid residues PHE308, PHE155, ALA276, THR 219, ASP347, ARG310 and ASN239. More importantly, strong alkyl interactions emerged from PHE175 to the methyl group and LEU216 to the other methyl group of grifolamine A, as well as carbon hydrogen bonds formed between the oxygen in the carbonyl group grifolamine A and amino acid residues PHE309, PRO307 and HIE237, may further stabilize the complexes. In a word, molecular docking revealed that grifolamine A docked into the hydrophobic cavity of  $\alpha$ -glucosidase and might alter the micro-structure of  $\alpha$ -glucosidase by different interactions, and eventually decrease the activity of  $\alpha$ -glucosidase.

### 3.6. MD simulation and free energy calculation and decomposition

Compared to molecular docking, MD simulation could provide a more comprehensive view to reveal the dynamic behavior and mechanism of interaction systems deeply (Tian et al., 2022). In order to examine the interaction between grifolamine A and  $\alpha$ -glucosidase precisely, we performed an MD simulation. The RMSD, which measured the stability of the ligand-enzyme complex was depicted in Fig. 8. The complex converged equilibrium after 35 ns. Hence, MD simulations by MM/GBSA were employed to calculate the average binding free energies. 5000 snapshots, extracted from the stable stages of the trajectory were calculated. The results showed that the binding free energy of  $\alpha$ -glucosidase with grifolamine A was  $-25.2 \pm 3.2 \text{ kcal/mol}$  averagely, which authenticated the high affinity and perfect dynamics of grifolamine A to  $\alpha$ -glucosidase.

Energy decomposition was then conducted to gain energy contributions of each residue. Apparently, the highlighted favorable amino acid residues were PHE155, LEU216, ASN239, PHE298, PHE308, PHE309, and ARG310 at the binding pocket (Fig. 9), indicating these

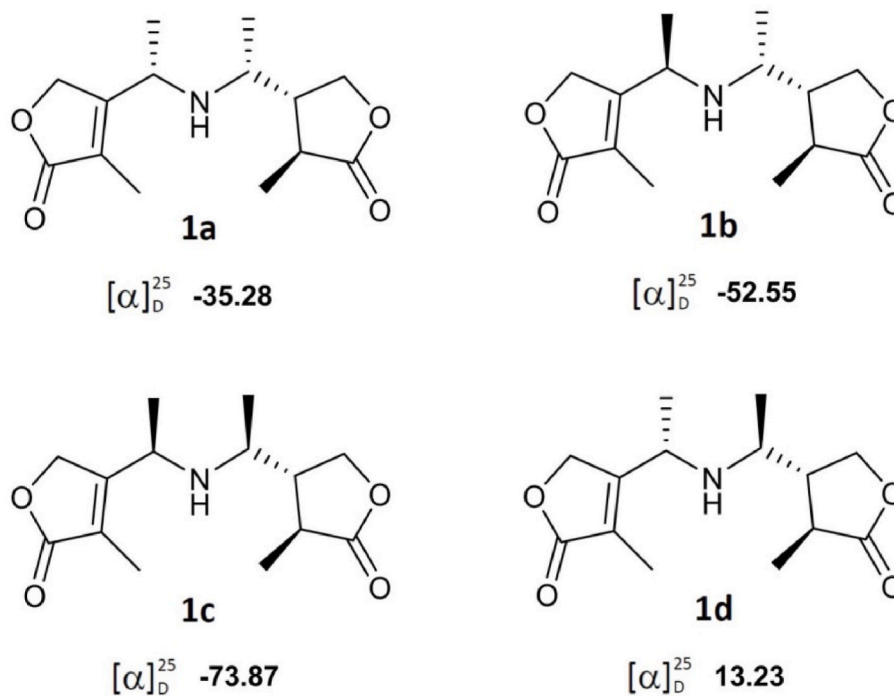
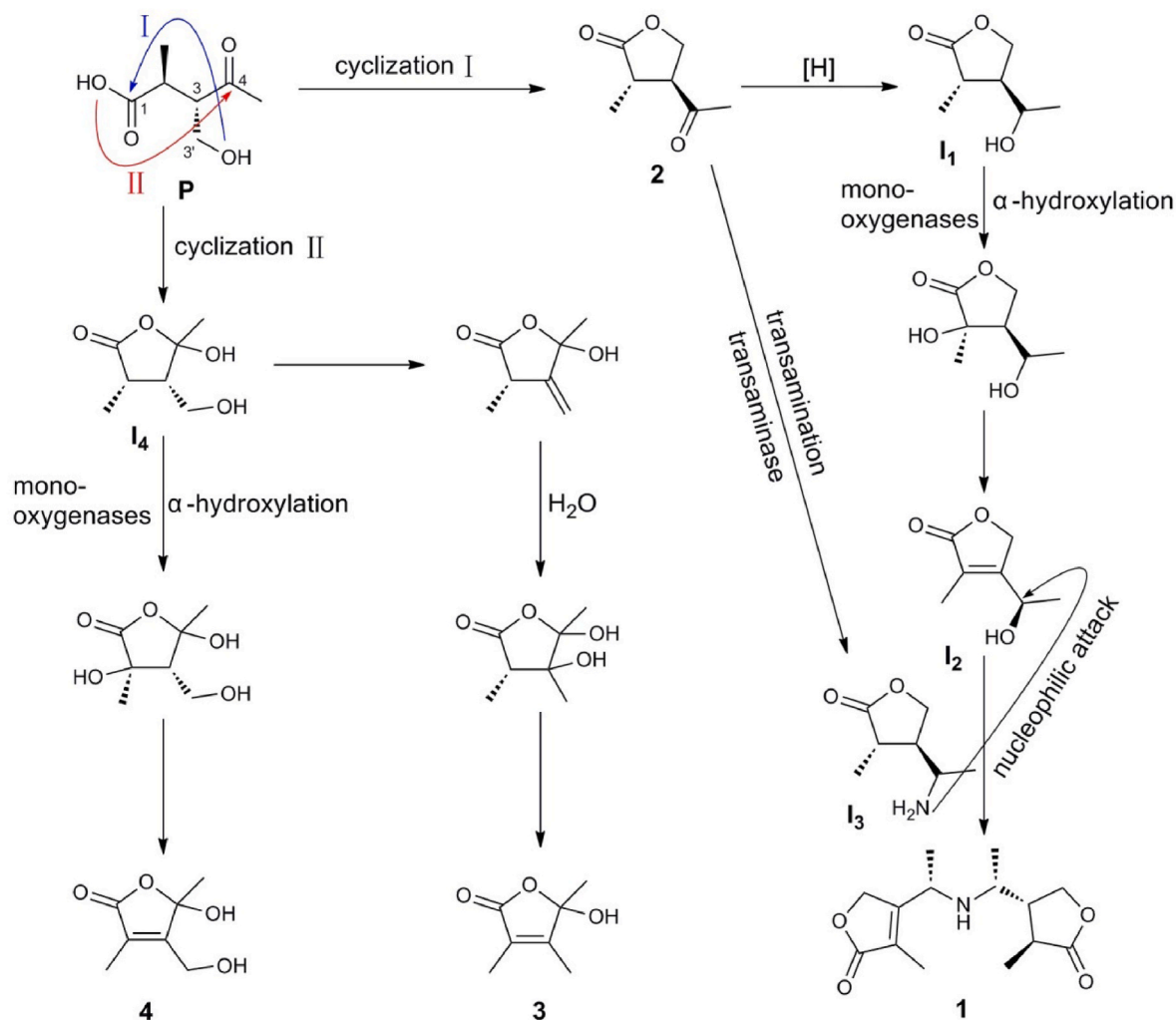


Fig. 5. Calculated specific optical rotations of 1a-1d.



Scheme 1. A proposed biogenetic origin of 1–4.

Table 1  
 $\alpha$ -Glucosidase inhibitory activity of compounds 1–4 ( $IC_{50}$ ,  $\mu$ M).

compounds	$\alpha$ -glucosidase from yeast	$\alpha$ -glucosidase from rats
1	78.6 $\pm$ 6.7	83.7 $\pm$ 4.4
2	192.9 $\pm$ 13.1	>100
3	>250	>100
4	>250	>100
acarbose	656.7 $\pm$ 17.3	32.1 $\pm$ 4.6

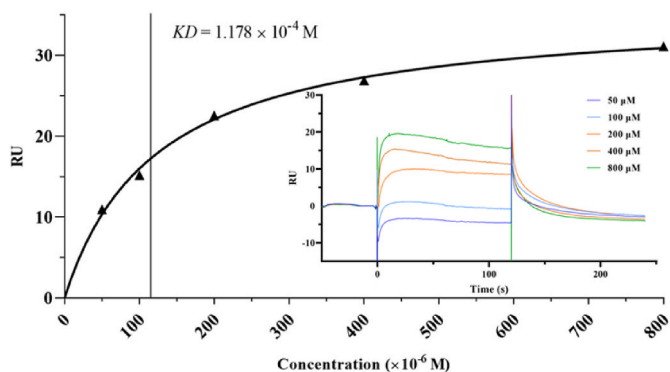
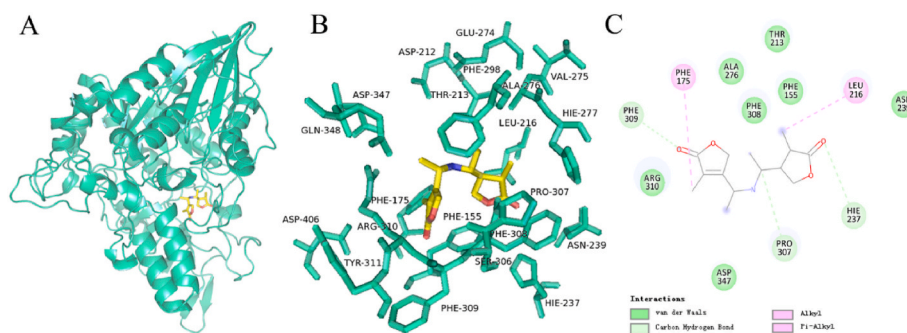


Fig. 6. SPR analysis.

amino acid residues had an importantly positive impact on the binding process. However, such amino acid residues as ASP212, GLU274, and ASP374 presented an adverse effect. Future work could be focused on the chemical modification of these key amino acid residues to verify the credibility of the molecular docking and MD modeling results.

#### 4. Conclusions

A novel bis- $\gamma$ -butyrolactone with N-linkage, the first natural  $\gamma$ -butyrolactone dimer named grifolamine A (1), together with three known  $\gamma$ -butyrolactone monomers (2–4) was isolated from the byproduct from *G. frondosa* polysaccharides preparation process. The stereochemistry and postulated biosynthetic origin of grifolamine A (1) were established. Grifolamine A exhibited a potentially inhibitory effect against  $\alpha$ -glucosidase. SPR manifested grifolamine A strongly affinity to  $\alpha$ -glucosidase with an equilibrium dissociation constant ( $K_D$ ) value of  $1.178 \times 10^{-4}$  M. Molecular docking manifested that grifolamine A bound to the active site of  $\alpha$ -glucosidase and changed the structure of  $\alpha$ -glucosidase by van der Waals force, alkyl interaction and carbon hydrogen bonds. MD simulation revealed that grifolamine A had high binding affinity to  $\alpha$ -glucosidase with average free energy of  $-25.2 \pm 3.2$  kcal/mol, which was in accordance with the results of SPR. Free energy decomposition indicated amino acid residues including PHE298, PHE308, PHE309, PHE155 and ARG310 at the binding pocket played strongly positive effect on the interaction between grifolamine A and  $\alpha$ -glucosidase. Overall, our findings provide new insight on the design



**Fig. 7.** Molecular docking conformations and interactions between yeast  $\alpha$ -glucosidase and grifolamine A (1) (A) Conformation of the binding of grifolamine A (1) towards  $\alpha$ -glucosidase; (B) Interactions of grifolamine A (1) to key residues of  $\alpha$ -glucosidase; (C) 2D scheme of interactions of grifolamine A (1) to key residues of  $\alpha$ -glucosidase.

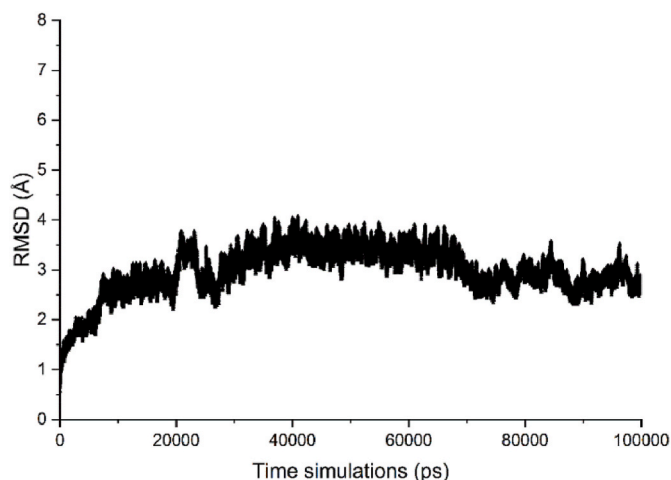


**Fig. 8.** Time dependence of root mean square deviation (RMSD) of the backbone atoms for  $\alpha$ -glucosidase in the complex.

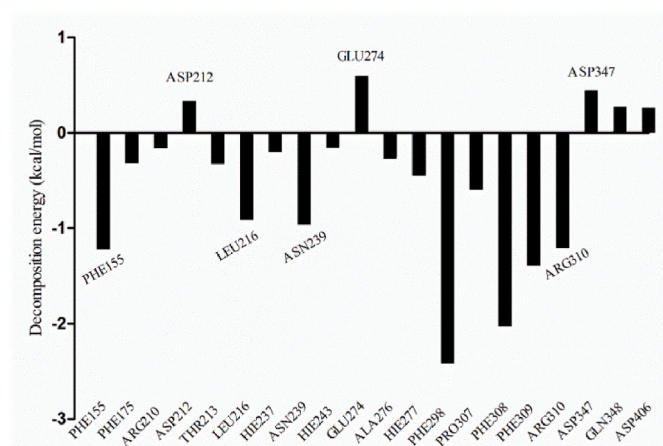


**Fig. 9.** Decomposition of binding free energy of each residue for  $\alpha$ -glucosidase.

and development of novel  $\alpha$ -glucosidase inhibitors based on  $\gamma$ -butyrolactone skeleton. Future work will focus on the therapeutic effect of grifolamine A on T2DM and the underlying mechanism *in vivo*.

#### CRediT authorship contribution statement

**Shaodan Chen:** Methodology, Writing – original draft, Writing – review & editing, Funding acquisition. **Zhenqiang Mu:** Methodology,

Writing – review & editing, Funding acquisition. **Tianqiao Yong:** Data curation, Funding acquisition. **Jiangyong Gu:** Methodology. **Yifan Zhang:** Resources. **Xiong Gao:** Writing – review & editing. **Yizhen Xie:** Supervision. **Chun Xiao:** Supervision. **Huiping Hu:** Supervision. **Xiaobing Yang:** Funding acquisition. **Xiangmin Li:** Supervision. **Manjun Cai:** Supervision. **Qingping Wu:** Project administration, Funding acquisition.

#### Declaration of competing interest

The authors declare that they have no known competing financial interests or personal relationships that could have appeared to influence the work reported in this paper.

#### Acknowledgements

We are grateful to Prof. Huajie Zhu, from Hebei University, China, for the guidance on the stereochemical structure identification and the calculated experiments. This work was financially supported by National Natural Science Foundation of China (81803393, 31901696), Guangdong Basic and Applied Basic Research Foundation (2020A1515011337), Guangdong Province Science and Technology Project (2019A050520003), GDAS' Project of Science and Technology Development (2022GDASZH-2022010101), Guangdong Province Agriculture Research Project & Agricultural Technique Promotion Project (2022KJ103) and Natural Science Foundation of Chongqing (cstc2019cyj-msxmX0780).

#### Appendix A. Supplementary data

Supplementary data to this article can be found online at <https://doi.org/10.1016/j.crfs.2022.10.026>.

#### References

- Aldeghi, M., Heifetz, A., Bodkin, M.J., Knappd, S., Biggin, P.C., 2016. Accurate calculation of the absolute free energy of binding for drug molecules. *Chem. Sci.* 7 (1), 207–218.
- Araujo, N.M.P., Arruda, H.S., Farias, D.d.P., Molina, G., Pereira, G.A., Pastore, G.M., 2021. Plants from the genus *Eugenia* as promising therapeutic agents for the management of diabetes mellitus: a review. *Food Res. Int.* 142, 110182.
- Bobst, A.M., 1984. Circular dichroic spectroscopy-Exciton coupling in organic stereochemistry-Harada, N, Nakanishi, K. J. *Am. Chem. Soc.* 106 (20), 6121–6122.
- Cao, Y., Fang, J., Shi, Y., Wang, H., Chen, X., Liu, Y., Zhu, Z., Cao, Y., Hong, Z., Chai, Y., 2022. Screening potential P-glycoprotein inhibitors by combination of a detergent-free membrane protein extraction with surface plasmon resonance biosensor. *Acta Pharm. Sin. B* 12 (7), 3113–3123.
- Chen, S., Lin, B., Gu, J., Yong, T., Gao, X., Xie, Y., Xiao, C., Zhan, J.Y., Wu, Q., 2022. Binding interaction of betulinic acid to  $\alpha$ -glucosidase and its alleviation on postprandial hyperglycemia. *Molecules* 27 (8), 2517.
- Chen, S., Yong, T., Xiao, C., Gao, X., Xie, Y., Hu, H., Li, X., Chen, D., Pan, H., Wu, Q., 2021. Inhibitory effect of triterpenoids from the mushroom *Inonotus obliquus* against  $\alpha$ -glucosidase and their interaction: inhibition kinetics and molecular stimulations. *Bioorg. Chem.* 115, 105276.

- Chen, S., Yong, T., Xiao, C., Su, J., Zhang, Y., Jiao, C., Xie, Y., 2018. Pyrrole alkaloids and ergosterols from *Grifola frondosa* exert anti- $\alpha$ -glucosidase and anti-proliferative activities. *J. Funct. Foods* 43, 196–205.
- Choi, J., Suzuki, T., Okumura, H., Noguchi, K., Kondo, M., Nagai, K., Hirai, H., Kawagishi, H., 2014. Endoplasmic reticulum stress suppressive compounds from the edible mushroom *Mycoleptodonoides aitchisonii*. *J. Nat. Prod.* 77 (7), 1729–1733.
- Fang, Y., Yang, M., Cai, L., Wang, J., Yin, T., Yu, J., Ding, Z., 2018. New phenylpropanoids from *Bulbophyllum retusiusculum*. *Arch. Pharm. Res. (Seoul)* 41 (11), 1074–1081.
- Forzato, C., Furlan, G., Nitti, P., Pitacco, G., Marchesan, D., Coriani, S., Valentin, E., 2005. A combined experimental and computational strategy in the assignment of absolute configurations of 4-methyl-5-oxo-tetrahydrofuran-3-carboxylic acids and their esters. *Tetrahedron Asymmetry* 16 (18), 3011–3023.
- Forzato, C., Nitti, P., Pitacco, G., 1997. Bicyclic gamma-butyrolactones. Relation between conformation of the lactone ring and chiroptical properties. *Tetrahedron Asymmetry* 8 (24), 4101–4110.
- Kumari, R., Kumar, R., Lynn, A., Open Source Drug Discovery, C., 2014. g\_mmpbsa-A GROMACS tool for high-throughput MM-PBSA calculations. *J. Chem. Inf. Model.* 54 (7), 1951–1962.
- LaPlante, S.R., Bilodeau, F., Aubry, N., Gillard, J.R., O'Meara, J., Coulombe, R., 2013. N-versus O-alkylation: utilizing NMR methods to establish reliable primary structure determinations for drug discovery. *Bioorg. Med. Chem. Lett.* 23 (16), 4663–4668.
- Li, N., Gao, X., Pan, Y., Liu, B., Pang, J., Zhao, C., Zeng, F., 2022. Effects of alkaloid-rich extracts obtained from *Grifola frondosa* on gut microbiota and glucose homeostasis in rats. *Food Funct.* 13 (5), 2729–2742.
- Liao, Y., Liu, X., Yang, J., Lao, Y.Z., Yang, X.W., Li, X.N., Zhang, J.J., Ding, Z.J., Xu, H.X., Xu, G., 2015. Hypersubones A and B, new polycyclic acylphloroglucinols with intriguing adamantane type cores from *Hypericum subsessile*. *Org. Lett.* 17 (5), 1172–1175.
- Luis Ros, J., Francini, F., Schinella, G.R., 2015. Natural products for the treatment of type 2 diabetes mellitus. *Planta Med.* 81 (12–13), 975–994.
- Meng, M., Cheng, D., Han, L., Chen, Y., Wang, C., 2017. Isolation, purification, structural analysis and immunostimulatory activity of water-soluble polysaccharides from *Grifola Frondosa* fruiting body. *Carbohydr. Polym.* 157, 1134–1143.
- Miao, L., Liu, C., Cheong, M.S., Zhong, R., Tan, Y., Rengasamy, K.R.R., Leung, S.W.S., Cheang, W.S., Xiao, J., 2022. Exploration of natural flavones' bioactivity and bioavailability in chronic inflammation induced-type-2 diabetes mellitus. *Crit. Rev. Food Sci. Nutr.* <https://doi.org/10.1080/10408398.2022.2095349>.
- Mizuno, M., Sakane, I., Minato, K., Watanabe, J., Hashimoto, T., 2017. Hot water extract of *Grifola gargal* possesses anti-inflammatory activity. *Food Sci. Technol. Res.* 23 (5), 725–732.
- Okuda, T., Kiyomoto, A., Harigaya, S., 1964. Studies on optical rotatory dispersion of 5-membered sugar-lactones-Configuration sign of optical rotatory dispersion curve. *Chem. Pharmaceut. Bull.* 12 (4), 504–506.
- Ouyang, Y., Nie, J., Gao, X., Zhao, C., 2022. *Grifola frondosa* polysaccharide ameliorates hyperglycemia and gut microbiota in type 2 diabetic mice. *Free Radic. Biol. Med.* 180, 65–65.
- Silverstein, R.M., Webster, F.X., Kiemle, D.J., 2005. *Spectrometric Identification of Organic Compounds*, 7 ed. John Wiley & Sons, Inc.
- Srinivasan, J., Cheatham, T.E., Cieplak, P., Kollman, P.A., Case, D.A., 1998. Continuum solvent studies of the stability of DNA, RNA, and phosphoramidate - DNA helices. *J. Am. Chem. Soc.* 120 (37), 9401–9409.
- Sun, L., Miao, M., 2020. Dietary polyphenols modulate starch digestion and glycaemic level: a review. *Crit. Rev. Food Sci. Nutr.* 60 (4), 541–555.
- Surmont, R., Verniest, G., De Kimpe, N., 2010. Short synthesis of the seed germination inhibitor 3,4,5-trimethyl-2(5H)-furanone. *J. Org. Chem.* 75 (16), 5750–5753.
- Suttithumsatid, W., Shah, M.A., Bibi, S., Panichayupakaranant, P., 2022. Alpha-Glucosidase inhibitory activity of cannabidiol, tetrahydrocannabinol and standardized cannabinoid extracts from *Cannabis sativa*. *Curr. Res. Food Sci.* 5, 1091–1097.
- Tian, X., Rao, L., Zhao, L., Wang, Y., Liao, X., 2022. Multispectroscopic and computational simulation insights into the inhibition mechanism of epigallocatechin-3-gallate on polyphenol oxidase. *Food Chem.* 393.
- Xu, H., Jiang, N., Guo, Y., Jiao, R.H., Cui, J.T., Song, Y.C., Tan, R.X., 2011. Fully substituted unsaturated lactones from endophytic *Myrothecium* sp. *J. Asian Nat. Prod. Res.* 13 (11), 1003–1007.
- Yaoita, Y., Ishizuka, T., Kakuda, R., Machida, K., Kikuchi, M., 2000. Structures of new ceramides from the fruit bodies of *Grifola frondosa*. *Biol. Pharm. Bull.* 23 (9), 1356–1358.
- Zhang, A., Deng, J., Yu, S., Zhang, F., Linhardt, R.J., Sun, P., 2018. Purification and structural elucidation of a water-soluble polysaccharide from the fruiting bodies of the *Grifola frondosa*. *Int. J. Biol. Macromol.* 115, 221–226.
- Zhang, J., Liu, D., Wen, C., Liu, J., Xu, X., Liu, G., Kan, J., Qian, C., Jin, C., 2022. New light on *Grifola frondosa* polysaccharides as biological response modifiers. *Trends Food Sci. Technol.* 119, 565–578.
- Zhu, H., 2009. *Current Organic Stereochemistry*. Science Presses of China.
- Zhu, H., 2015. *Organic Stereochemistry-Experimental and Computational Methods*. Wiley-VCH, Verlag GmbH & Co. KGaA.